Int. J. Nano Dimens., 11 (2): 177-187, Spring 2020

ORIGINAL ARTICLE

Study of multilayer and multi-component coatings deposited using cathodic Arc technique on H-13 hot work steel for die-casting applications

Rajesh Mundotia[1,2,], Tatyarao Ghorude[1], Ashwin Kale[2], Umesh Mhatre[2]*

[1] *Department of Physics, N B Mehta Science College, Bordi, Palghar-401701, India*
[2] *Surface Modification Technologies Pvt. Ltd, Vasai (East), Maharashtra: 401 208, India*

Received 29 January 2020; revised 29 March 2020; accepted 31 March 2020; available online 14 April 2020

Abstract

Die casting process is used since long, but even today problems like erosion, corrosion, soldering and sticking affect die life. These dies undergo thermal cyclic loads from 70 oC to 600 oC during processing. Physical Vapor Deposition (PVD) hard coating can play an important role in such extreme applications. In the present work, we report the use of Chromium based multilayer CrN/Cr (M-CrN) coatings and multi-component aluminium titanium based AlTiN (M-AlTiN) coatings. The H-13 steel substrate samples were prepared using cathodic arc deposition technique. Structural properties of the coated samples were studied using XRD and SEM techniques. Tribological and mechanical properties of the coatings were studied using Calo-test and Micro-hardness test respectively. Potentiostat technique was used to study the effect of 1 M HCl solution on these coatings. Thermal fatigue (TF) test was conducted by heating the sample to around 600 oC and rapidly cooling it to room temperature imitating the die casting process conditions. After multiple cycles, it was observed that M-AlTiN coated samples outperform M-CrN coated samples in terms of wear, oxidation and adhesion properties. It was observed that formation of oxide layer on the coated surface during the thermal cycling inhibits further oxidation of the coating layer and result in enhanced productivity and efficiency of dies.

Keywords: *Coating Adhesion; Die Casting Application; H-13 Hot Work Steel; PVD Coatings; Thermal Fatigue; Wear Rate.*

How to cite this article

Mundotia R, Ghorude T, Kale A, Mhatre U. Study of multilayer and multi-component coatings deposited using cathodic Arc technique on H-13 hot work steel for die-casting applications. Int. J. Nano Dimens., 2020; 11 (2): 177-187.

INTRODUCTION

High pressure die casting (HPDC) is a fast and reliable method for high precision castings with complex shapes. The process offers mass production of plastic, rubber and light alloy components within the acceptable quality at competitive prices [1]. In this process, molten material is injected in the cavity at high velocities i.e., 60 m/s. This high velocity enhances the density of the product but cause substantial wear of the die due to erosion [2]. When the molten material is aluminum alloy, it contains Si and other abrasive particles which could deteriorate die surface and affect the product quality. Also, the molten aluminum readily reacts with tool steel causing soldering, corrosion and sticking [3]. Other major factor which can affect the process is thermal fatigue. During each cycle, molten metal is injected inside the mold and then cooled within the order of few milliseconds. These thermal-mechanical loadings cause thermal stress and dimensional variation. The thermal fatigue failure can be characterized by the network of small cracks on the die surface after a sufficient number of cyclic thermal and mechanical loading. All these factors can affect the production efficiency and quality [4].

Most appropriate metallurgy for such

* Corresponding Author Email: *rajeshmundotia@gmail.com*

application is H-13 steel (Cr 4.75-5.5, Mo 1.1-1.75, Si 0.8-1.2, V 0.8-1.2, C 0.32-0.45, Ni 0.3, Cu 0.25, Mn 0.2 - 0.5, P 0.03, S 0.03) which is widely used in hot work applications [5]. The general term hot work tool corresponds to the steels used above 200 ^{o}C temperature. In addition to usual working stresses, these steels undergo thermal stress as they come in contact with hot material. These steels delay occurrence of heat check marks resulting due to frequent temperature changes at the surface. To avoid hot cracks (tension cracks) developing far inside into the tools, hot working steels need to have high temperature toughness. For tools which undergo high stress, impact or pressure at elevated temperatures, special attention is required for high strength. Any change in structure at elevated temperatures could results in reduction of material strength. Hence, high strength, stability and retention of hardness at elevated temperature is required. Therefore, H-13 steel was used as substrate. Other critical demands included resistance to high temperature wear, corrosion, oxidation and soldiering. To accomplish these demands, various surface treatments like lubricants, surface nitriding, shot penning, electroplating, Physical Vapor Deposition (PVD) coating etc. were introduced [4,6-10]. Conventionally, Cr electroplating on such tool is well known to provide solutions to such glitches. Due to plating de-lamination during thermal cycling and stringent environmental regulation a more sustainable alternative like PVD coating [7] is required.

Various studies had been carried out on PVD coatings for such applications [1, 2, 8-11]. But there is still a need to understand vital properties like structure, oxidation, wear resistance and adhesion of the coating after thermal fatigue [12-16]. Authors have reported contradictory results in their studies e.g. F. Fazlalipour *et al.* [12] found that nano-structured coatings not only act as a physical and chemical barrier to prevent atomic diffusion and intermetallic phase formation but also reduce wettability and adhesion between steel and molten aluminum alloy. Luigi Avico *et al.* [13] characterized Cr-based and Ti-based multilayer and single layer PVD coatings in terms of both corrosion behavior and surface properties for mold technology applications. They observed that TiN monolayer coating exhibited superior corrosion resistance compared to other Cr-based multilayer coatings. M. Okumiya and M. Gripentrog [14] in their study discussed that the multilayer structure reduces the coating lifetime due to poor adhesion of the coating but S. Paldey and S.C. Deevi [15] found that multilayer structure results in improved hardness and strength.

Jose Mario Paiva *et al.* [8] studied high temperature tribological and wear properties of nanocomposite coatings prepared using pulsed cathodic arc evaporation. Die casting molds, core pin and blocks were coated and studied under usual production conditions. Aneta Wilczek *et al.* [16] studied arc deposited nano-multilayer coatings for molds. The microstructure, mechanical and wear properties of the coated samples were analyzed. In both cases, effect of thermal cycles on coating properties were not carried out. Therefore, it is essential to understand coating properties after thermal fatigue which is the most prominent cause of die failure.

The aim of present work was to characterize PVD coatings for die casting application, in terms of structural, tribology, mechanical, corrosion, oxidation and adhesion properties. To understand the effects Chromium based multilayer coating (M-CrN) and multi-component Aluminium Titanium based coating (M-AlTiN) were deposited on hardened H-13 substrate. Coating structure, surface morphology, micro-hardness and corrosion properties of the sample were studied. Thermal fatigue test was carried out on uncoated as well as coated samples. These samples were further analyzed to obtained structural variations, oxidation, wear rate and adhesion properties. The results obtained would clearly specify the failure of the samples undergone thermal fatigue and performance of the different coating structure for such application.

EXPERIMENTAL PROCEDURE

Sample preparation

To conduct this study, hardened H-13 hot work steel as substrate (Φ 25 mm x 8 mm, 53-54 HRC) was used. These substrates were polished to a surface finish of R_a = 0.015 **±** 0.002 **µm**. The substrates were ultrasonically cleaned vigorously in alkaline solution and then rinsed with DI water before oven drying for 30 min. Samples were then loaded on rotating carousel in Cathodic Arc Physical Vapor Deposition (CA-PVD) vacuum chamber. After achieving a base vacuum of 8.0 x 10^{-3} Pa, the samples were etched (in situ cleaning) with Cr ions in pure Ar gas. Before coating, a Cr

Table 1. Deposition parameters used to prepare CA-PVD coating samples.

Deposition parameter	M-CrN coating	M-AlTiN
Targets used	Cr	Ti and AlTi (67:33)
Ion etching, bias and time	Cr, -900V & 5 min	Ti, -900V & 5 min
Arc current	Cr at 60 Amp	Ti at 60 & AlTi at 70 Amp
Deposition pressure	1.3 Pa	3 Pa
Deposition temperature	350°C	450°C
Bias Voltage	-100 ± 10 V	-100 ± 10 V
Coating structure	CrN/Cr multilayer	AlTiN/TiN multilayer

bond layer was deposited to improve adhesion. This was followed by CrN layer deposited using ultra-high pure N_2 gas for 4 min. By Switching Ar and N_2 gases, CrN/Cr multi-layered (15/14 layers) coating was deposited. Similarly, for M-AlTiN coating, the samples were etched with Ti ions. TiN adhesive layer was deposited at -150 V bias for 4 min. Multilayers of AlTiN and TiN were deposited by simultaneously using both AlTi and Ti targets in N_2 gas pressure of 3 Pa. The carousel speed was kept at 3 rpm. Similar technique was used to deposit multilayered structure by various authors [9, 10]. Thicker final layer of CrN and AlTiN coating was deposited for M-CrN and M-AlTiN coating respectively. For structural analysis coating was deposited on Si substrate. The deposition parameters of the coatings are mentioned in Table 1.

Characterizations

For coating phase analysis G-XRD was performed using Rigaku (Ultima –IV) X-ray diffractometer with Cu Kα radiation source and a goniometer in a Bragg–Brentano configuration at scan rate of 2°/min.

Thickness and wear rate of the M-CrN and M-AlTiN coating were measured using calo-test method. Wear rate measurement method were based on Rutherford model [17]. Abrasive diamond ultrafine particles suspended in distilled water (20 wt.%) was fed at the interface. Five craters with different sliding distance were created on each sample for 240, 180, 120, 60 and 30 sec durations. After calo-test, the craters were observed under optical microscope at 50x magnification to measure the crater size. Using crater diameter wear coefficient was calculated. Higher wear co-efficient corresponds to higher wear rate.

Coating hardness was measured using Fischerscope HM-2000 at 20mN load. Measurements were done using loading and unloading curves based on Oliver and Pharr method [18].

Corrosion tests were performed using Digi-Ivy DY2300 series potentiostat with three-electrode cell consisting of a graphite counter electrode, a saturated calomel reference electrode (SCE) and the studied specimens as the working electrode. The electrolyte used was 1.0 M HCl solution prepared in double distilled water at room temperature. The potentiostat was used in linear sweep voltammetry (LSV) mode and varied from -0.7 to 0 volt in steps of 5 mV/Sec. E_{corr} and I_{corr} values were measured using tafel plot. Corrosion rate was calculated using faraday law in mm/yr. [19].

Coating adhesion with the substrate was studied using scratch adhesion test for quantitative results and Mercedes adhesion test for qualitative results. Scratch adhesion test were carried out using DUCOM Scratch Tester TR-101 on the coated samples in ramp mode (by progressive incremental) load from 30 to 60 N at speed of 0.2 mm/sec. Total scratch length was fixed to 10 mm. Critical failure loads (failure onset) of the coating adhesion were identified by abrupt rise in frictional force data and also can be verified by observing the scratch under the optical microscope [20]. Mercedes adhesion test was carried out using Rockwell hardness tester at 150 Kgf load and standard diamond tip having 200 **µm** (±10 µm) tip radius. The indentation was observed under microscope and classified as per VDI 3198 standards [21].

For thermal fatigue test (TF), samples were placed in a preheated furnace at 850 °C for 73 secs resulting in surface temperature of 600°C and then dipped in the water at room temperature for 20 secs. This procedure of thermal fatigue test was adopted from Guobin *et al*., [5] to imitate the die casting process. The samples subjected to thermal fatigue cycling for 100, 300 and 400 times were named as TF100, TF300 and TF400 respectively. Samples without thermal fatigue treatment were named as TF0. After test, thermal cracks and

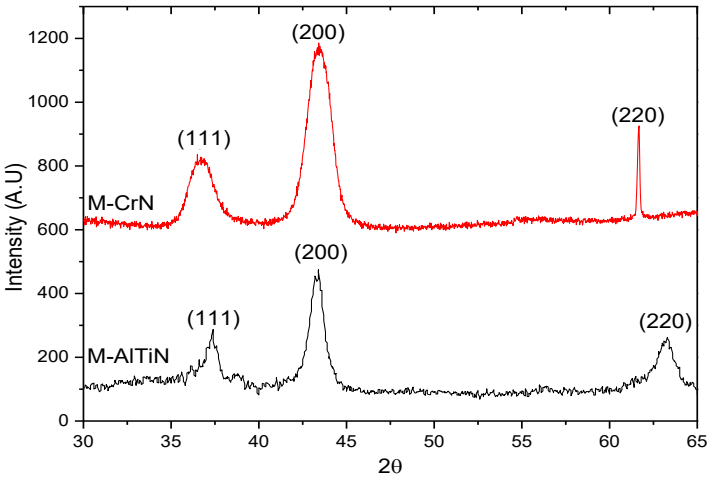

Fig. 1. XRD plots of M-CrN and M-AlTiN coating deposited on Si substrate.

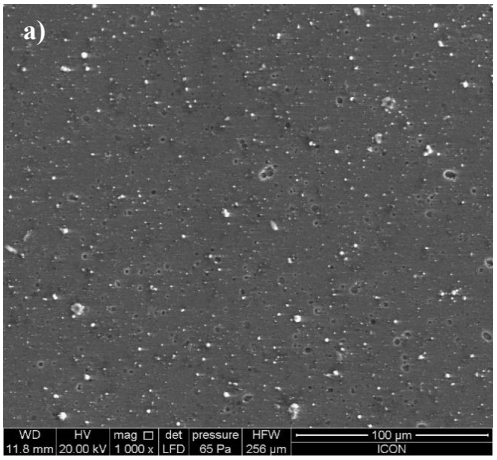

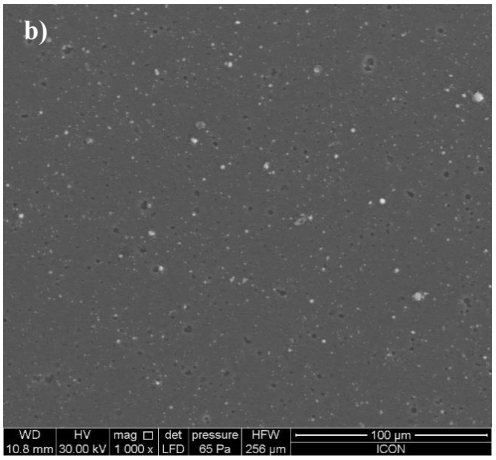

Elements	Cr	N
at. %	58.88	41.12

Elements	Al	Ti	N
at. %	42.30	28.77	28.93

Fig. 2. SEM images of a) M-CrN and b) M-AlTiN coating with elemental composition measured using EDAX analysis.

coating chip-off if any was examined under the optical microscope. Coating structure, oxidation, wear rate and adhesion of the thermally cycled samples were studied using XRD, calo-test and scratch test respectively.

RESULTS AND DISCUSSION

XRD analysis

Fig. 1 shows XRD pattern of M-CrN and M-AlTiN coating. It was observed that for both M-CrN and M-AlTiN coatings, FCC phase was formed with (200) as prominent growth orientation. Formation of cubic CrN and cubic AlTiN phase was confirmed from XRD plot. We did not observe any hexagonal phase of CrN or AlN. This means that the hexagonal phases either do not exist or their content is too low to be detected by the XRD technique [1].

SEM with EDAX analysis

Fig. 2 shows SEM images of coated samples along with their elemental composition (Fig. 2). More surface defects like droplets and pinholes were visible in case of M-CrN coating (Fig. 2a) compared to M-AlTiN coating (Fig. 2b). Less surface defects in coating structure improves the corrosion and wear resistance properties as

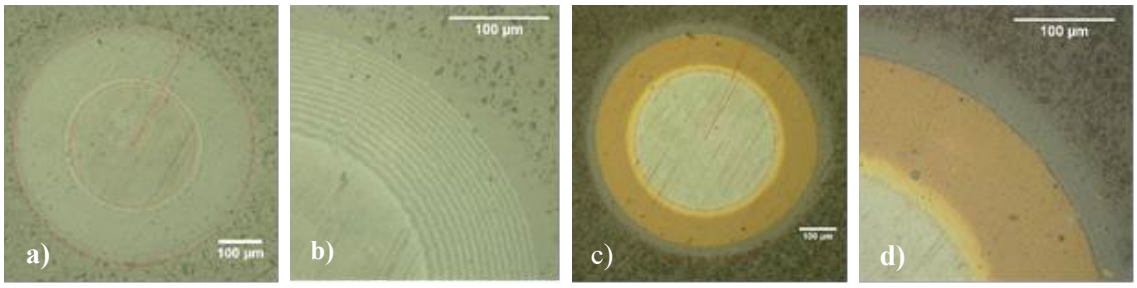

Fig. 3. Crater images of a) M-CrN Coating at 50x, b) M-CrN Coating at 200x, c) M-AlTiN Coating at 50x, d) M-AlTiN Coating at 200x taken using optical microscope.

CrN final layer	0.7 µm
CrN/Cr multilayer (14/14 layers)	2.0 µm
Cr adhesive layer	0.1 µm
H-13 Substrate	

M-CrN Coating structure

(a)

AlTiN final layer	1.0 µm
AlTiN/TiN multilayer	2.0 µm
TiN adhesive layer	0.3 µm
H-13 Substrate	

M-AlTiN coating structure

(b)

Fig. 4. Schematic representation of (a) M-CrN and (b) M-AlTiN coating structures with each layer thickness details.

observed by S. Abusuilik [22]. In case of M-AlTiN coating, Al:Ti composition ratio was found to be 60:40 whereas target (cathode) composition was 67:33 (Fig. 2b). Lower Al content observed in EDAX study could be result of high bias (100V) during M-AlTiN deposition.

Coating thickness, wear rate and micro-hardness measurements

Calo test was performed on the M-CrN (Fig. 3a, 3b) and M-AlTiN (Fig. 3c, 3d) coated H-13 samples. The schematic representation of layer structure and thickness measured using calo-test is shown in fig.4 (a, b). In case of M-CrN coating (Fig. 4a), intermediate layer thickness was around ~70 nm. In case of M-AlTiN coating (Fig.4.b), no multilayer structure was observed. Cr layer was used as adhesive layer for M-CrN coating and TiN layer for M-AlTiN coating. This inter layer is important to reduce the lattice mismatch between the substrate and coating leading to a lower epitaxial stress component and a flatter stress gradient at the interface [23].

Wear rate of the uncoated H-13, M-CrN and M-AlTiN coated samples were studied. It was observed that, wear rate of the uncoated samples was higher compared to coated samples. M-AlTiN coating display the lowest wear rate compared to other samples (Table 2). Less defects, higher hardness and dense coating structure of M-AlTiN coating reduces abrasive wear.

Fig. 5 (a, b) shows the micro hardness measurements for M-CrN and M-AlTiN coated samples. The measurements were performed at 20 mN load. The depth of indentation was well under 10% of the coating thickness. Micro-hardness values are mentioned in Table 2. The measurements show that M-AlTiN coating exhibit high hardness compared to M-CrN coating.

Accelerated corrosion study using potentiostat

M-CrN and M-AlTiN coated H-13 samples were exposed to 1.0 M HCl solution. Tafel plot results of uncoated H-13, M-CrN and M-AlTiN are shown in Fig. 6. It was observed that coated samples exhibited better corrosion resistance than uncoated substrate (Table 3). M-AlTiN coating shows better corrosion resistance than M-CrN coating. More number of interfaces and dense defect free coating structure of M-AlTiN coating

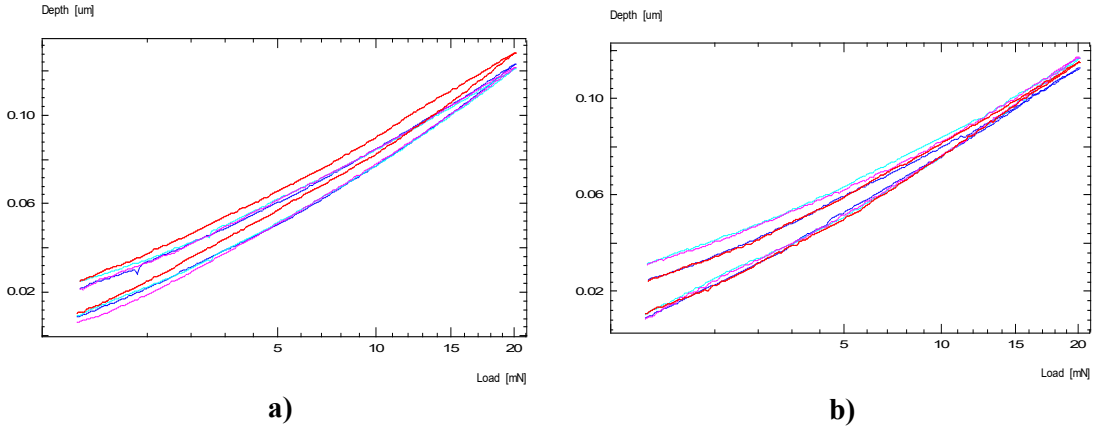

Fig. 5. Loading unloading curves of micro-hardness test carried out on a) M-CrN Coating and b) M-AlTiN Coating deposited on H-13 hardened substrate.

Table 2. Thickness, wear rate and hardness properties of various samples.

Coating properties	Thickness	Wear rate	Hardness
Uncoated	NA	5.15 x 10^{-14} m^2/N	589 HV (54 HRC)
M-CrN coating	2.8 µm	4.66 x 10^{-14} m^2/N	2720 $HV_{0.02}$
M-AlTiN coating	3.3 µm	2.44 x 10^{-14} m^2/N	3089 $HV_{0.02}$

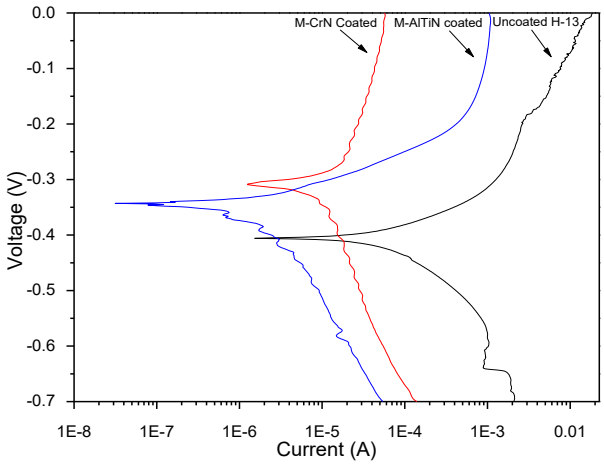

Fig. 6. Tafel plots of uncoated, M-CrN coated and M-AlTiN coated H-13 substrate tested in 1.0 M HCl corrosive solution at ambient temperature.

Table 3. Corrosion rate, E_{corr} and I_{corr} values of various samples calculated using Tafel plot.

Sample details	Corrosion Rate (mm/yr)	E_{corr} (V)	I_{corr} (A)
Uncoated H-13	9.988 x 10^{-1}	-0.406	8.616 x 10^{-5}
M-CrN coated	1.408 x 10^{-1}	-0.307	1.215 x 10^{-5}
M-AlTiN coated	2.242 x 10^{-2}	-0.341	1.934 x 10^{-6}

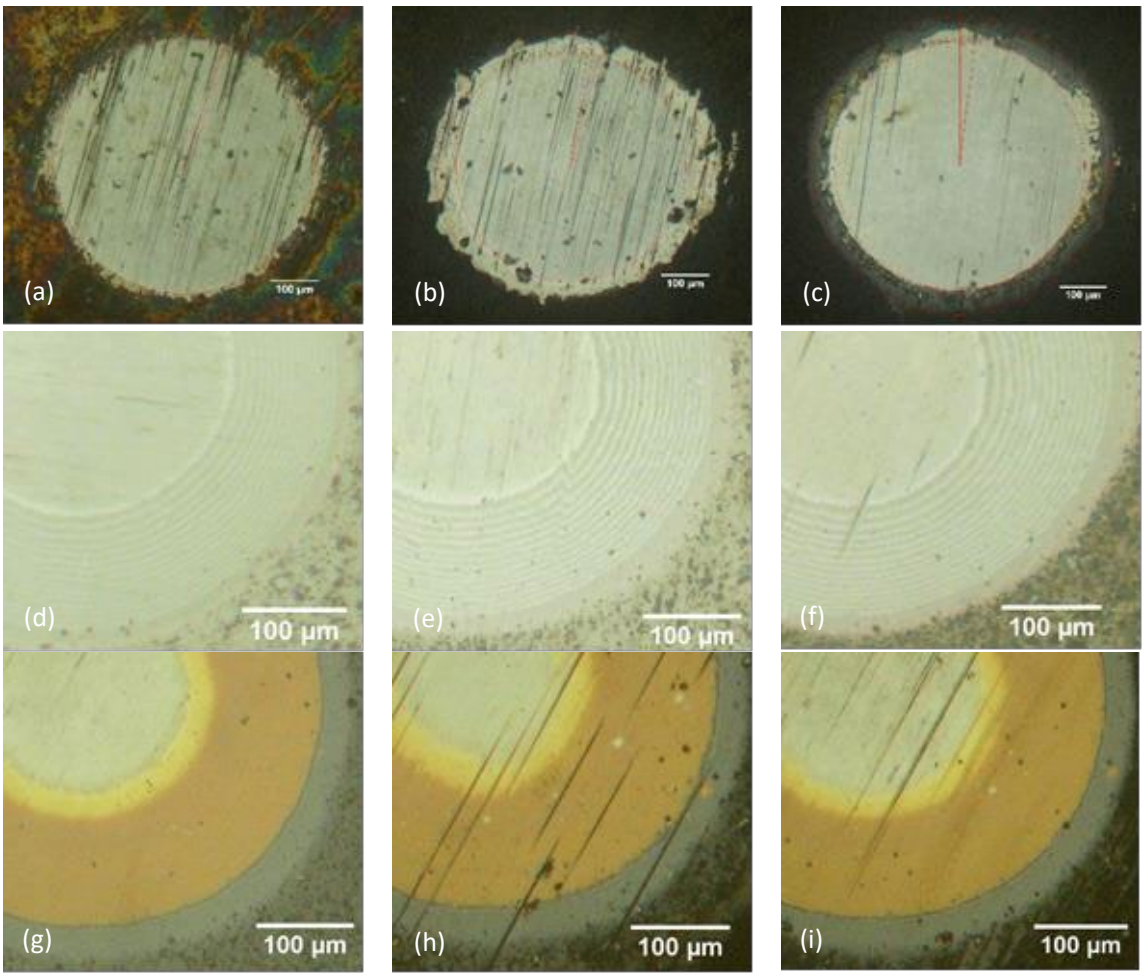

Fig. 7. Crater images of Uncoated H-13 (a, b, c), M-CrN coated (d, e, f) and M-AlTiN coated (g, h, i) samples subjected to TF100, TF300 and TF400 cycles respectively.

could be the reason behind better inertness to corrosive medium. Nevertheless, M-CrN coating had less negative corrosion potential compared to M-AlTiN coating. Therefore, for die casting application, coatings can effectively enhance the corrosion resistance properties and can reduces deterioration of die and mold surface.

Thermal Fatigue test

Uncoated as well as coated H-13 samples were subjected to thermal fatigue (TF) cycles for 100, 300 and 400 times. No thermal fatigue cracks were observed for all the samples which confirm that duly heat-treated H-13 steel can withstand the thermal-mechanical loading [5]. For uncoated samples after TF, oxide layer was clearly visible in the crater images and thickness increases with more TF cycles (Fig.7a, 7b, 7c). Oxide layer thickness measured was 0.4 µm, 1.1 µm and 1.57 µm with TF100, TF300 and TF400 respectively. Similar method was used by N. Thorat *et al.*, [24] to measure the oxide layer thickness of monolayer $Al_xTi_{1-x}N$ coating. For coated sample, no variation was observed after TF100 (Fig.7d, 7g) but very fine surface oxide was formed (not measurable using calo-test). In case of TF300 and TF400 discoloration of sample surface was observed (Fig.7e, 7f, 7h, 7i). No oxide layer ring was observed for coated samples as seen in case of uncoated samples (Fig.7a, 7b, 7c). This clearly shows the advantage of PVD coated surface over the uncoated surface.

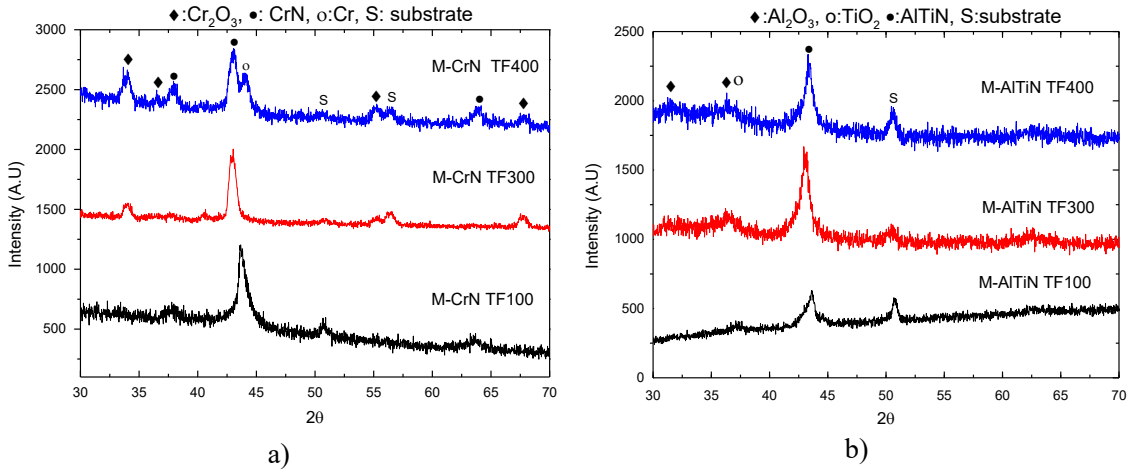

Fig. 8. XRD plots of a) M-CrN and b) M-AlTiN coating deposited on H-13 substrate subjected to TF100, TF300 and TF400 cycles.

Table 4. Wear rate of samples subjected to different thermal fatigue cycles.

Sample Details	Wear rate against diamond slurry after Thermal fatigue cycles (m^2/N)			
	TF0	TF100	TF300	TF400
Uncoated H-13	5.15×10^{-14}	6.78×10^{-14}	8.53×10^{-14}	9.81×10^{-14}
M-CrN coated	4.06×10^{-14}	4.38×10^{-14}	4.51×10^{-14}	4.78×10^{-14}
M-AlTiN coated	2.44×10^{-14}	2.86×10^{-14}	2.97×10^{-14}	3.38×10^{-14}

XRD measurements after thermal fatigue test

XRD analysis done on thermal fatigue samples revealed formation of oxides on M-CrN (Fig. 8a) coating and M-AlTiN (Fig. 8b) coating [25-28]. But oxygen diffusion after TF cycles was restricted to surface for both the coated samples as observed in optical images (Fig. 7). In case of M-CrN coated samples, Cr_2O_3 oxide peaks appears after TF 100 and becomes clearly visible after TF400. In case of M-AlTiN coated samples, TiO_2 peaks appears after TF100 whereas Al_2O_3 oxide peaks appear for TF300 samples, not much change in peaks intensity was observed for TF400 samples. Formation of Al_2O_3 layer on the surface reduces further oxygen diffusion within the coating structure and also reduces out diffusion of Ti towards surface. Therefore, oxidation resistance of M-AlTiN coated samples is better compared to other samples.

Wear rate measurements after thermal fatigue test

Wear rate of the samples with and without TF were examined against diamond slurry using Calo-wear (Table. 4). For all samples, the wear rate increase with increase in TF cycles. But increase in wear rate of the uncoated H-13 samples was rapid compared to coated samples (Fig. 9). Formation of soft oxide layer for uncoated samples deteriorates surface wear resistance property and results in increased wear rate. In case of coated samples, very thin layer of surface oxides was formed (Fig. 7) after thermal fatigue and not much variation in wear rate was observed. For dies which undergo thermal cycling, surface coating plays an important role in reducing abrasion and corrosion.

Scratch and Mercedes adhesion test after thermal fatigue test

Fig. 10 shows scratch adhesion test results of the M-CrN and M-AlTiN coated samples after TF cycling. It was observed that coating adhesion improved after TF cycles for both coatings. Diffusion of intermediate layer during TF cycles could have resulted in improvement in the adhesion properties [29]. This needs further investigation. In Mercedes adhesion test, all the samples were found to be in the acceptable range of adhesion (Table. 5). In case of M- CrN coated sample (Fig.11a-d), the adhesion improves from HF3 to HF2 after TF cycles. In case of M-AlTiN

Fig. 9. Bar graph representation of wear rate for uncoated H-13, M-CrN coated and M-AlTiN coated samples subjected to TF0, TF100, TF300 and TF400 cycles.

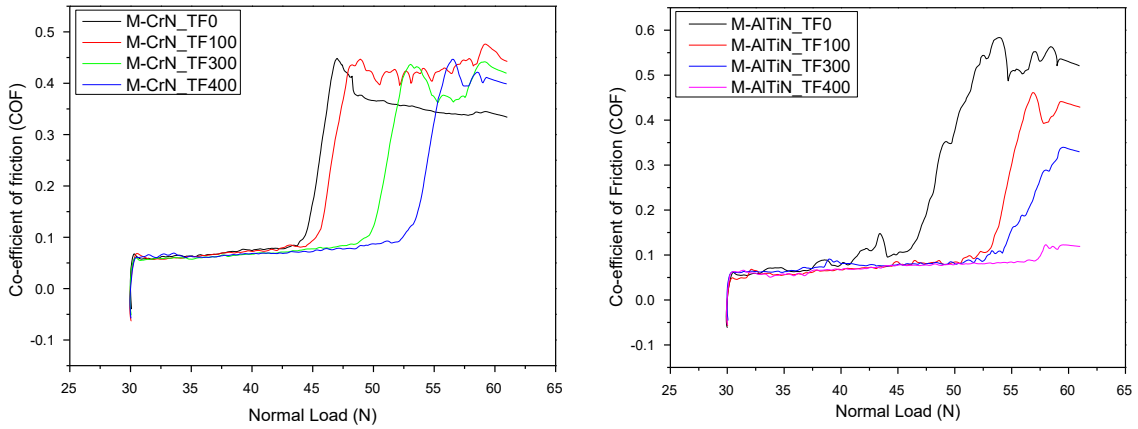

Fig. 10. Comparison of scratch adhesion test results of a) M-CrN and b) M-AlTiN coated H-13 samples subjected to different thermal fatigue cycles.

Table 5. Scratch and Mercedes adhesion test results of coated samples subjected to different thermal fatigue cycles.

Sample details	M-CrN samples with different TF				M-AlTiN samples with different TF			
	TF0	TF100	TF300	TF400	TF0	TF100	TF300	TF400
Failure Load (N)	44	46	51	53	46	53	54	58
Mercedes test	HF3	HF2	HF2	HF2	HF1	HF1	HF1	HF1

samples (Fig.11e-h), a fine brittle oxide layer of Al_2O_3 was formed for TF400 sample which chips-off after Mercedes test but the lower coating structure remains intact.

CONCLUSION

From this study, it was clear that the PVD coating improves various properties like wear resistance, oxidation resistance and corrosion

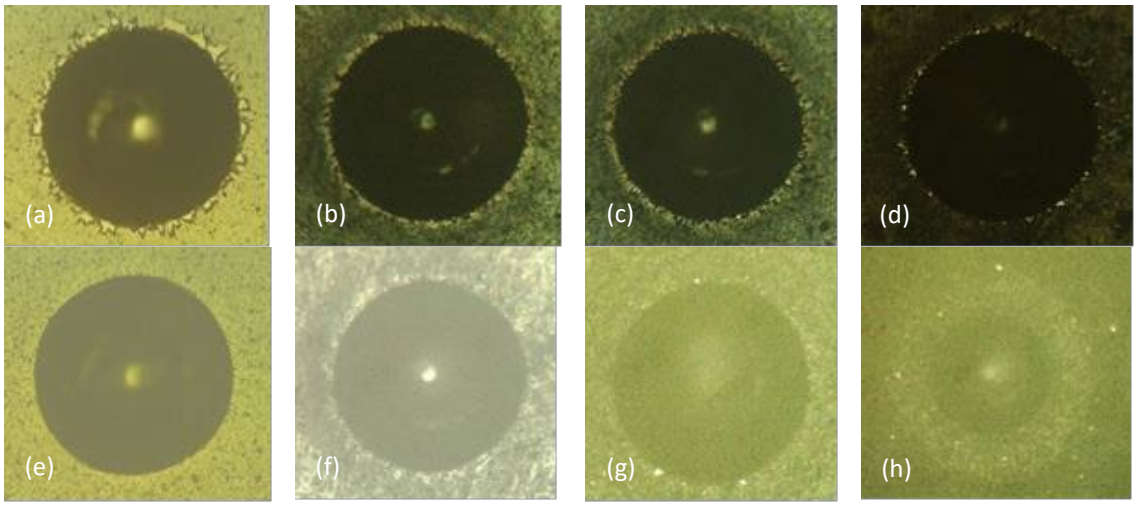

Fig. 11. Indentation images of the Mercedes adhesion test carried out on M-CrN coating (a, b, c, d) and M-AlTiN coating (e, f, g, h) on H-13 substrate subjected to TF0, TF100, TF300 and TF400 cycles respectively.

resistance. Therefore, application of such multilayer and multi-component coating can reduce machine down time, enhance productivity and product quality. It was concluded that,

- FCC CrN phase for M-CrN coating and AlTIN phase for M-AlTiN coating was formed with (200) as prominent orientation.
- SEM images revealed fewer defects in M-AlTiN coating compared to M-CrN coating.
- Multilayer structure of CrN and Cr was observed in M-CrN coating whereas mixed layer of AlTiN and TiN was observed in case of M-AlTiN.
- M-AlTiN coating proved to be better compared to M-CrN in terms of tribological, mechanical, adhesion and corrosion resistance properties.
- After TF cycling thermal cracks were not observed in any samples.
- After TF cycling, thick oxide layers were formed in case of uncoated samples and its thickness was found to be increasing with TF cycles. Whereas very thin surface oxide layer (not observable in crater edges) for coated samples was confirmed using XRD measurement.
- Wear resistance property of the uncoated samples deteriorate rapidly with TF cycles whereas for coated samples, it was marginal.
- Scratch test showed increase in adhesion with increase in number of TF cycles. It could be due to diffusion of intermediate bond layer during TF cycling.

Results show that multi-layer PVD coating do not get crack formation even after thermal fatigue cycles. These coatings can help improve the life of dies by protecting it from erosion, corrosion, sticking and soldiering in severe conditions.

ACKNOWLEDGEMENT

Authors acknowledges Surface Modification Technologies Pvt. Ltd (SMTPL) India for providing the hard coating samples and allowing to use their research and development lab facilities for analysis.

CONFLICT OF INTEREST

The authors declare that they have no competing interests.

REFERENCES

[1] Kovacevic L., Terek P., Miletic A., Kukuruzovic D., Koric B., Panjan P., (2018), Industrial evaluation of duplex PVD hard coatings for HPDC. *J. Braz. Soc. Mech. Sci. Eng.* 40: 271-278.

[2] Mitterer C., Holler F., Ustel F., Heim D., (2000), Application of hard coatings in aluminium die casting soldering, erosion and thermal fatigue behaviour. *Surf. Coat. Technol.* 125: 233–239.

[3] Sundqvist M., Hogmark S., (1993), Effects of liquid aluminium on hot-work tool steel. *Tribol. Int.* 26, issue 2: 129-134.

[4] Liu B., Wang B., Yang X., Zhao X., Qin M., Gu J., (2019), Thermal fatigue evaluation of AISI H13 steels surface modified by gas nitriding with pre- and post-shot peening. *Appl. Surf. Sci.* 483: 45–51.
[5] Li G., Li X., Wu J., (1998), Study of the thermal fatigue crack initial life of H13 and H21 steels. *J. Mater. Process. Technol.* 74: 23–26.
[6] Wang B., Zhao X., Li W., Qin M., Gu J., (2018), Effect of nitrided-layer microstructure control on wear behavior of AISI H13 hot work die steel. *Appl. Surf. Sci.* 431: 39-43.
[7] Legg K. O., Graham M., Chang P., Rastagar F., Gonzales A., Sartwell B., (1996), The replacement of electroplating. *Surf. Coat. Technol.* 81: 99-105.
[8] Paiva J. M., Fox-Rabinovich G., Locks Junior, E., Stolf P., Seid Ahmed Y., Matos Martins M., Bork C., Veldhuis S., (2018), Tribological and wear performance of nanocomposite PVD hard coatings deposited on aluminum die casting tool. *Materials.* 11: 358-363.
[9] Peng J., Zhu Z., Su D., (2019), Sliding wear of nitrided and duplex coated H13 steel against aluminium alloy. *Tribol. Int.* 129: 232-238.
[10] Wang B., Bourne G. R., Korenyi-Both A. L., Monroe A. K., Midson S. P., Kaufman M. J., (2016), Method to evaluate the adhesion behavior of aluminum-based alloys on various materials and coatings for lube-free die casting. *J. Mater. Process. Technol.* 237: 386-393.
[11] Bobzin K., Brögelmann T., Brugnara R. H., Kruppe N. C., (2015), CrN/AlN and CrN/AlN/Al_2O_3 coatings deposited by pulsed cathodic arc for aluminum die casting applications. *Surf. Coat. Technol.* 284: 222-229.
[12] Fazlalipour F., Naghashnejan M., Nushari M. N., (2019), Evaluation of adhesion and erosion/corrosion resistance of Nano-composite and Nano-multilayer thin films in molten aluminum alloy. *SN Appl. Sci.* 1: 1308-1313.
[13] D'Avico L., Beltrami R., Lecis N., Trasatti S. P., (2019), Corrosion behavior and surface properties of PVD coatings for mold technology applications. *Coatings.* 9: 7-14.
[14] Okumiya M., Gripentrog M., (1999), Mechanical properties and tribological behavior of TiN–CrAlN and CrN–CrAlN multilayer coatings. *Surf. Coat. Technol.* 112: 123–128.
[15] Paldey S., Deevi S. C., (2003), Single layer and multilayer wear resistant coatings of (Ti,Al)N: A review. *Mater. Sci. Eng: A.* 342: 58-79.
[16] Wilczek A., Morgiel J., Rogal Ł., Maziarz W., Smolik J., (2020), Microstructure and wear of (CrN/CrAlN)/(CrAlN/VN) and (CrN/TiAlN)/(TiAlN/VN) coatings for molds used in high pressure casting of Aluminum. *Coatings.* 10: 261-272.
[17] Rutherford K. L., Hutchings I. M., (1996), A micro-abrasive wear test, with particular application to coated systems. *Surf. Coat. Technol.* 79: 231-239.
[18] Oliver W. C., Pharr G. M., (1992), An improved technique for determining hardness and elastic modulus using load and displacement sensing indentation experiments. *J. Mater. Res.* 7: 1564-1583.
[19] Mundotia R., Thorat N., Kale A., Mhatre U., Kothari D. C., Kovacs T., Ghorude T., (2019), Study of corrosion properties of CrN and multilayer CrN/Cr coating at different electrolyte temperatures deposited on stainless steel by vacuum arc process. *AIP Conf. Proceed.* 2115: 030313.
[20] Bull S. J., Berasetegui E. G., (2006), An overview of the potential of quantitative coating adhesion measurement by scratch testing. *Tribol. Int.* 39: 99–114.
[21] Vidakis N., Antoniadis A., Bilalis N., (2003), The VDI 3198 indentation test evaluation of a reliable qualitative control for layered compounds. *J. Mater. Process. Technol.* 143–144: 481–485.
[22] Abusuilik Saleh B., (2015), Pre-intermediate, and post-treatment of hard coatings to improve their performance for forming and cutting tools. *Surf. Coat. Technol.* 284: 384-395.
[23] Schönjahn C., Ehiasarian A. P., Lewis D. B., New R., Münz W.-D., Twesten R. D., Petrov I., (2001), Optimization of in situ substrate surface treatment in a cathodic arc plasma: A study by TEM and plasma diagnostics. *J. Vac. Sci. Technol. A.* 19: 1415-1420.
[24] Thorat N., Mundotia R., Varma R., Kale A., Mhatre U., Patel N., (2018), Structural & oxidation behavior of TiN & $Al_xTi_{1-x}N$ coatings deposited by CA-PVD technique. *AIP Conf. Proceed.* 1942: 080041.
[25] Chim Y. C., Ding X. Z., Zeng X. T., Zhang S., (2009), Oxidation resistance of TiN, CrN, TiAlN and CrAlN coatings deposited by lateral rotating cathode arc. *Thin Solid Films.* 517: 4845–4849.
[26] Conde A., Cristóbal A. B., Fuentes G., Tate T., Damborenea J. De., (2006), Surface analysis of electrochemically stripped CrN coatings. *Surf. Coat. Technol.* 201: 3588–3595.
[27] Wu Z. T., Qi Z. B., Zhu F. P., Liu B., Wang Z. C., (2013), Influences of Y addition on mechanical properties and oxidation resistance of CrN coating. *Phys. Proced.* 50: 150 – 155.
[28] Barshilia H. C., Jain A., Rajam K. S., (2004), Structure, hardness and thermal stability of nanolayered TiN/CrN multilayer coatings. *Vacuum.* 72: 241–248.
[29] Brooks J. S., Davidson J. L., Forder S. D., Munz W. D., Larsson M., (1997), A Mossbauer spectroscopy study of Ti–Fe interfaces produced by the PVD process. *Thin Solid Films.* 308–309: 351–357.